LANGMUIR Article
Cite This: Langmuir 2018, 34, 13713−13724
pubs.acs.org/Langmuir

pH-Dependent Adsorption Release of Doxorubicin on MamC-Biomimetic Magnetite Nanoparticles

Germán García Rubia,[†] Ana Peigneux,[†] Ylenia Jabalera,[†] Javier Puerma,[†] Francesca Oltolina,[§] Kerstin Elert,[‡] Donato Colangelo,[§] Jaime Gómez Morales,[∥] Maria Prat,[§] and Concepcion Jimenez-Lopez*[,†]

[†]Departamento de Microbiología, and [‡]Departamento de Mineralogía y Petrología, Facultad de Ciencias, Universidad de Granada, Campus de Fuentenueva S/N, 18002 Granada, Spain

[§]Dipartimento di Scienze della Salute, Università del Piemonte Orientale "A. Avogadro", Via Solaroli 17, 28100 Novara, Italy

[∥]Laboratorio de Estudios Cristalográficos, IACT (CSIC-Universidad de Granada), Avda. Las Palmeras, 4, 18100 Armilla, Spain

ABSTRACT: New biomimetic magnetite nanoparticles (hereafter BMNPs) with sizes larger than most common superparamagnetic nanoparticles were produced in the presence of the recombinant MamC protein from *Magnetococcus marinus* MC-1 and functionalized with doxorubicin (DOXO) intended as potential drug nanocarriers. Unlike inorganic magnetite nanoparticles, in BMNPs the MamC protein controls their size and morphology, providing them with magnetic properties consistent with a large magnetic moment per particle; moreover, it provides the nanoparticles with novel surface properties. BMNPs display the isoelectric point at pH 4.4, being strongly negatively charged at physiological pH (pH 7.4). This allows both (i) their functionalization with DOXO, which is positively charged at pH 7.4, and (ii) the stability of the DOXO−surface bond and DOXO release to be pH dependent and governed by electrostatic interactions. DOXO adsorption follows a Langmuir−Freundlich model, and the coupling of DOXO to BMNPs (binary biomimetic nanoparticles) is very stable at physiological pH (maximum release of 5% of the drug adsorbed). Conversely, when pH decreases, these electrostatic interactions weaken, and at pH 5, DOXO is released up to ∼35% of the amount initially adsorbed. The DOXO−BMNPs display cytotoxicity on the GTL-16 human gastric carcinoma cell line in a dose-dependent manner, reaching about ∼70% of mortality at the maximum amount tested, while the nonloaded BMNPs are fully cytocompatible. The present data suggest that BMNPs could be useful as potential drug nanocarriers with a drug adsorption-release governed by changes in local pH values.

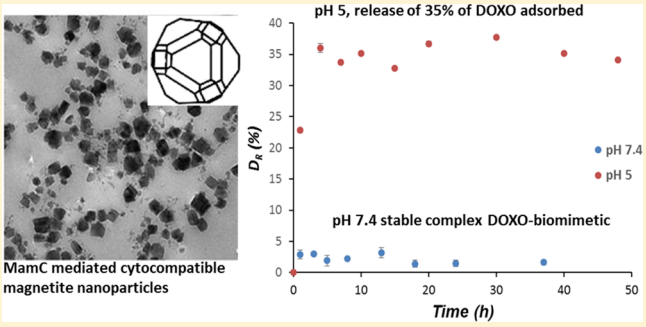

INTRODUCTION

One of the potential clinical applications of magnetic nanoparticles (MNPs) that is foreseen is their use as drug nanocarriers based on the fact that their movement can be controlled by an external magnetic field.[1−4] Several studies have shown that these nanoparticles exhibit low to no toxicity in humans due to their possible degradation in the liver and spleen, which results in the release of Fe^{3+} ions that participate in iron metabolism.[3] This represents an advantage compared to other delivery systems including ceramics, polymers, and metals, in which several drawbacks concerning their biodegradability, the toxicity of their degradation byproducts, or simply the toxicity of the nanoparticles have been hindering their clinical application.[5]

Although noticeable progress has been made regarding the use of MNPs in this context, concern still exists regarding their toxicity, and because of that, the doses of nanoparticles need to be the minimum possible to minimize the potential side effects arising during the clinical treatments. These concerns are derived from the fact that conventional synthesis of magnetic nanostructured materials often requires toxic reagents.[1] Moreover, the superparamagnetic nanoparticles resulting from these synthetic procedures are relatively small (<30 nm) and have large size distributions, which limit the magnetic moment per particle and thus their efficiency in responding to an external magnetic field. Finally, most of the synthetic procedures used so far to produce these nanoparticles are usually expensive since they usually involve extreme temperatures, strict reaction atmospheres, and, in many cases, time-consuming postsynthetic processing.[2]

On the contrary, biological magnetite nanocrystals produced by magnetotactic bacteria offer a greener alternative. These bacteria have the ability to produce magnetite nanoparticles (Fe_3O_4) by means of biologically controlled mineralization,

Received: September 12, 2018
Revised: October 19, 2018
Published: November 5, 2018

DOI: 10.1021/acs.langmuir.8b03109
Langmuir 2018, 34, 13713−13724

which consists of the production of intracellular magnetic crystals surrounded by a lipid bilayer, resulting in an organelle called magnetosome.[6] Magnetosomes, far larger than most inorganic magnetites produced at room temperature, are considered to be the ideal magnetic nanoparticles, and, consequently, these are the most demanded nanoparticles in many nanotechnological applications.[2] On the one hand, they present higher cytocompatibility, probably favored by the presence of a phospholipid membrane around them that could also improve functionalization and cell internalization.[1,7] On the other hand, they have almost perfect crystal structures, well-defined morphologies, and narrow size distributions, features far superior compared to those of synthetic MNPs.[1,2] All these features make them single magnetic domain nanoparticles of fairly large size and thus with the largest magnetic moment per particle.[2,8,9] This is important since the low magnetization per particle of smaller chemically synthesized magnetic nanoparticles makes it difficult to effectively direct their movement with moderate external magnetic fields, thus reducing the efficiency of a directed chemotherapy.[9,10]

Moreover, the larger size enhances the heating capacity of the magnetosomes with respect to that usually obtained when using chemically synthesized nanoparticles, thus allowing a reduction in the doses of magnetic material needed to heat a biological tissue.[1] Therefore, due to their large volumes, magnetosomes have a higher hyperthermia response (i.e., produce a larger amount of heat) compared to that of chemically synthesized nanoparticles when they are exposed to an alternating magnetic field. This has been shown for bacterial magnetosomes mixed in solution, which were either contained within the magnetotactic bacteria or extracted from these bacteria, and for magnetosomes arranged in chains or forming individual nanoparticles.[1,11]

Magnetosomes could reach the tumor by enhanced permeability and retention (EPR) effect because their size is ≤150 nm.[12] These authors showed a strong accumulation of magnetosomes from *Magnetospirillum magneticum* AMB-1 (mean typical length value of 45 nm) inside the tumor by EPR effect that persisted long after the complete washout of the nanoparticles from the blood vasculature. Moreover, they demonstrated a specific enhancement for RGD (Arginine, Glycine, Aspartic acid)-labeled magnetosomes (active targeting) compared to the unlabeled ones (passive-EPR effect).

Nowadays, the production of this type of nanoparticles to industrial levels is not pursued due to the slow growth of the magnetotactic bacteria and the difficulties associated with culturing them.[2] In this context, the biomimetic synthesis of magnetosome-like magnetite nanoparticles (BMNPs) mediated by magnetosome membrane-associated proteins has emerged as an alternative to produce a magnetosome-like nanoparticle without the need of culturing magnetotactic bacteria.[2] In particular, Mms6 from *M. magneticum* AMB-1 to a greater extent[8,13,14] and MamC from *Magnetococcus marinus* MC-1[15] are the magnetosome membrane-associated proteins that have been studied more thoroughly, so far, for the production of these biomimetic nanoparticles. These proteins control magnetite nucleation and/or growth, altering the size and/or the final morphology of these crystals, which, in turn, affect their magnetic properties. In the case of MamC-mediated magnetites, this material exhibits the highest blocking temperature and the slowest increase of magnetization compared to those of inorganic and/or Mms6-mediated magnetites, thus pointing to a larger magnetic moment per particle of MamC-mediated biomimetic magnetite nanoparticles.[15]

However, one of the drawbacks of most of the already commercialized inorganic magnetite nanoparticles is the need to coat their surface with different compounds (such as organic acids or polymers) to provide them with new chemical groups allowing functionalization, but possibly altering the magnetic properties of the magnetic nanoparticles.[2] In the present study, we will demonstrate that one of the advantages of using MamC-mediated BMNPs lies in the fact that MamC attaches to the BMNP surface and provides it with functional groups that allow functionalization based on electrostatic interactions. Moreover, the BMNPs used in this study are larger in size (30−40 nm) than conventional inorganic magnetites (<30 nm), thus allowing for a larger magnetic moment per particle while being superparamagnetic. This is important since they act as paramagnetic in the absence of an external magnetic field, thus preventing aggregation, while increasing the magnetic response, and thus the guidance efficiency, upon the application of an external magnetic field.

In addition, when dealing with cancer, as well as with other pathological conditions,[16] the differences in the pH values between healthy and diseased tissues can be exploited to control the chemotherapeutic agent release. Indeed, the microenvironment in tumor sites usually is more acidic (pH 5.8) than in healthy tissues and blood plasma (pH 7.4),[17] and it is even more acidic in lysosomes (pH 4−5) and endosomes (pH 5−6), in which magnetite nanocarriers could also be internalized.[17] In the present paper, we will also demonstrate that adsorption−desorption of the specific drug to BMNPs is activated by changes in the environmental pH values, that is, the physiological neutral pH of healthy tissue versus the acidic pH at tumor sites.

Doxorubicin (DOXO), an anthracycline antibiotic, was selected as the model chemotherapeutic agent[17−20] because of its wide spectrum of antitumor activity.[21] DOXO interferes in the DNA reparation process mediated by topoisomerase II and produces reactive oxygen species that damage cellular structures.[22,23] A major drawback associated with DOXO chemotherapy involves its significant severe side effects, concerning in particular cardiac function, and hepatic toxicity.[22,24] These nonspecific side effects could be dramatically reduced by the use of cytocompatible drug nanocarriers, and therefore the use of MamC-mediated BMNPs opens new perspectives in the clinical practice.

In this context, the present paper is the first work to explore the functionalization of MamC-mediated BMNPs with a chemotherapeutic agent and how the release of this drug could be easily controlled by varying the pH in *in vitro* experiments.

EXPERIMENTAL SECTION

Expression and Purification of MamC. The expression and purification of MamC as recombinant protein and the synthesis of MamC-mediated magnetite nanoparticles were carried out according to the procedure described previously.[15] MamC was expressed in *Escherichia coli* TOP10 (Invitrogen, Spain) after transformation with the plasmid pTrcHis-TOPO (Invitrogen, Spain) carrying the MamC protein coding gene (Mmc1_2265) coupled to a hexahistidine tag coding sequence at its 5′ terminus. Protein expression was induced with isopropyl-1-thio-β-D-galactopyranoside, and protein purification was carried out by fast protein liquid chromatography with an immobilized metal affinity chromatography. Then, MamC proteins

DOI: 10.1021/acs.langmuir.8b03109
Langmuir 2018, 34, 13713−13724

were refolded through dialysis, and their purity was evaluated by sodium dodecyl sulfate-polyacrylamide gel electrophoresis electrophoresis.

Synthesis of Inorganic Magnetite and MamC-Mediated BMNP Nanoparticles. The synthesis of purely inorganic magnetite nanoparticles (MNPs) was carried out at 25 °C and 1 atm total pressure from a solution containing 3.5 mM $NaHCO_3$, 3.5 mM Na_2CO_3, 2.78 mM $Fe(ClO_4)_2$, and 5.56 mM $FeCl_3$ at a pH value of 9. Similarly, the synthesis of MamC-mediated BMNPs was done by mixing the same aqueous solution added with 10 μg/mL of the recombinant MamC. All solutions were prepared from oxygen-free Milli-Q water deoxygenated by following the protocol described in Valverde-Tercedor.[15] Samples were incubated for 30 days. All experiments were performed inside an anaerobic COY chamber filled with an atmosphere of N_2 with 4% of H_2 to prevent magnetite oxidation. After the incubation period, the resulting magnetite nanoparticles were washed three times with deoxygenated Milli-Q water (50 mL). A set of MNPs and BMNPs was stored in 4-(2-hydroxyethyl)-1-piperazineethanesulfonic acid (HEPES) buffer (pH 7.4) inside the Coy Chamber until further analyses. Moreover, some of these BMNPs were autoclaved (121 °C, 15 min) with the goal of removing MamC (here referred to as BMNPs autoclaved), and, later, some of these nanoparticles were rinsed to further eliminate MamC (here referred to as BMNPs autoclaved rinsed). Another set of MNPs and BMNPs was suspended in citrate buffer (20 mg/mL) overnight with the goal of providing more functional groups that might facilitate the coupling and then rinsed and resuspended in HEPES buffer. These samples are here referred to as MNPs-citrate and BMNPs-citrate. Aliquots of 1 mL of BMNP-citrate nanoparticles (5 mg/mL) were exposed to UV light for 20 min. After that, the sample was treated with ultrapure N_2 to prevent potential magnetite oxidation. All samples were kept inside the COY chamber at 25 °C.

Nanoparticles Characterization. Powder X-ray diffraction (XRD) analysis was carried out with an Xpert Pro X-ray diffractometer (PANalytical; The Netherlands) using Cu Kα radiation, with the scan range set from 20 to 60° in 2θ (0.01°/step; 3 s per step). Identification of the precipitates was performed by using XPowder software.[25]

Transmission electron microscopy (TEM) analyses of nanoparticles were performed with a scanning transmission electron microscope Philips model CM20 microscope. Magnetic nanoparticles were embedded in Embed 812 resin. Ultrathin sections (50−70 nm) were prepared using a Reichert Ultracut S microtome (Leica Microsystems GmbH, Wetzlar, Germany) and deposited onto copper grids. The size of the crystals was measured using the ImageJ 1.47 program, and size distribution curves were determined from these measurements using Origin 8. To ensure reproducibility of results, particle sizes were measured on multiple micrographs with an accumulated amount of about 1000 nanoparticles measured for each experiment.

Magnetization measurements were carried out by using a quantum design superconducting quantum interference device 5T magnetic properties measurement system. Under gentle argon flow, 1.6 mg of MNPs and 1.01 mg of BMNPs were placed in a double-walled polycarbonate capsule. Hysteresis cycles for each type of nanoparticles were run at 5 and 300 K.

The stability of the samples was determined by means of recording the sedimentation process of the different nanoparticles (MNPs, BMNPs, BMNPs-UV, and DOXO−BMNPs). A volume of 0.5 mL, 5 mg/mL of these different nanoparticles in HEPES buffer, pH 7.4, was shaken in a vortex for 1 min and allowed to sediment. This was considered the time zero of the experiment. For each experiment type, the end of the sedimentation time was considered when a pellet forms at the bottom of the tubing.

The measurements of the hydrodynamic radius and electrophoretic mobility of the nanoparticles were performed at 25 °C in a Zetasizer Nano ZS instrument (Malvern Instruments, Instruments Ltd, U.K.) using disposable polystyrene cuvettes. The instrument uses the dynamic light scattering technique to provide a measurement of the particle size distribution of the nanoparticles in suspension. Additionally, it also incorporates a ζ-potential analyzer that uses electrophoretic light scattering and provides ζ-potential values, determined from electrophoretic mobility measurements, by applying Smoluchowski's mobility equation.[26]

Electrophoretic mobility was measured in inorganic magnetites and BMNPs, both uncoated and coated with citrate as well as in DOXO-loaded BMNPs (hereafter DOXO−BMNPs or binary biomimetic nanoparticles). Hydrodynamic radius was measured on MNPs-citrate, BMNPs-citrate, and DOXO−BMNPs. Stock suspensions of each type of the nanoparticles were prepared in 10 mL of oxygen-free $NaClO_4$ (10 mM). Aliquots of 200 μL of each stock were inoculated in eleven flasks, each one containing oxygen-free $NaClO_4$ 10 mM, with 10 mL being the final volume per flask. The pH of each one of the flasks was adjusted by adding oxygen-free HCl (0.1 M) or oxygen-free NaOH (0.1 M) to different pH values ranging from 2 to 11 depending on the sample. Samples were sonicated for 2 min before the measurements. Nine replicas were performed per measurement.

Thermogravimetric analyses (TGAs) were run on ∼10 mg of solid by heating the sample in an alumina cell under N_2 atmosphere at a rate of 20 °C/min up to a final temperature of 950 °C.

Nitrogen sorption isotherms of powdered samples were obtained at 77 K on a TriStar 3000 equipment (Micromeritics). About 50 mg of sample was degassed at 100 °C for 4 h prior to analysis using a sample degas system (VacPrep 061, Micrometrics). The surface area of the samples was determined using the Brunauer−Emmett−Teller (BET) method.[27]

DOXO Adsorption and Release. Doxorubicin hydrochloride (DOXO, $C_{27}H_{29}NO_{11}$·HCl) was purchased from Sigma-Aldrich. The molecular weight of the molecule without HCl is 543.52 g/mol. The kinetics of DOXO adsorption on BMNPs was carried out to determine the time needed to reach equilibrium. For these analyses, aliquots of the suspension of the BMNPs-citrate (5 mg) were added with 1 mL of DOXO (2 mM) in HEPES buffer (10 mM, 1 mL, pH 7.4). Mixtures were incubated at 25 °C for different time intervals, up to 48 h, under continuous mixing at 150 rpm in the dark to prevent DOXO photodegradation.[28] Then, DOXO−BMNPs, here referred to as binary biomimetic nanoparticles, were removed from the solution containing the nonadsorbed DOXO molecules by supercentrifugation at 10 000 rpm for 5 min. The pellets were washed twice with 1 mL of HEPES buffer, and all supernatants were measured by UV−vis spectroscopy at a wavelength of 480 nm. The amount of nonadsorbed DOXO (C_e) and the amount of adsorbed DOXO per mass unit of adsorbent (Q) were calculated from these measurements. The molar absorptivity of DOXO in HEPES buffer at 480 nm was determined as 9123.3 L/mol (R^2 = 0.9989) from the slope of a standard calibration straight line. More than three replicas were performed per experiment. The standard deviation of absorbance measurements was used to calculate the error in the DOXO concentration in the supernatant ($[DOXO]_{sn}$).

The adsorption isotherms were obtained by mixing 5 mg of BMNPs-citrate with 1 mL of different concentrations of DOXO, up to 7.4 mM, in HEPES buffer. More than 15 independent experiments were performed at equal or different initial concentrations of DOXO in the supernatant to build the adsorption isotherm. Experiments were replicated to ensure reproducibility. Mixtures were incubated at 25 °C for 3 h (time required to reach equilibrium, according to the adsorption kinetic). The data were fitted to the models of Langmuir and Langmuir−Freundlich (LF) by using Origin 8. The Langmuir adsorption model[29] considers that the surface is energetically homogeneous and the maximum adsorption surface occurs in a monolayer, without considering the possible interaction among the adsorbed drug molecules.[29,30] The Langmuir model is defined by eq 1, where Q is the amount of adsorbed drug per amount of nanoparticles, K_L is the Langmuir affinity constant, Q_{max} is the drug loading capacity, and C_e is the equilibrium concentration of drug in the supernatant.[29]

$$Q = \frac{Q_{max}(K_L C_e)}{1 + (K_L C_e)} \quad (1)$$

DOI: 10.1021/acs.langmuir.8b03109
Langmuir 2018, 34, 13713−13724

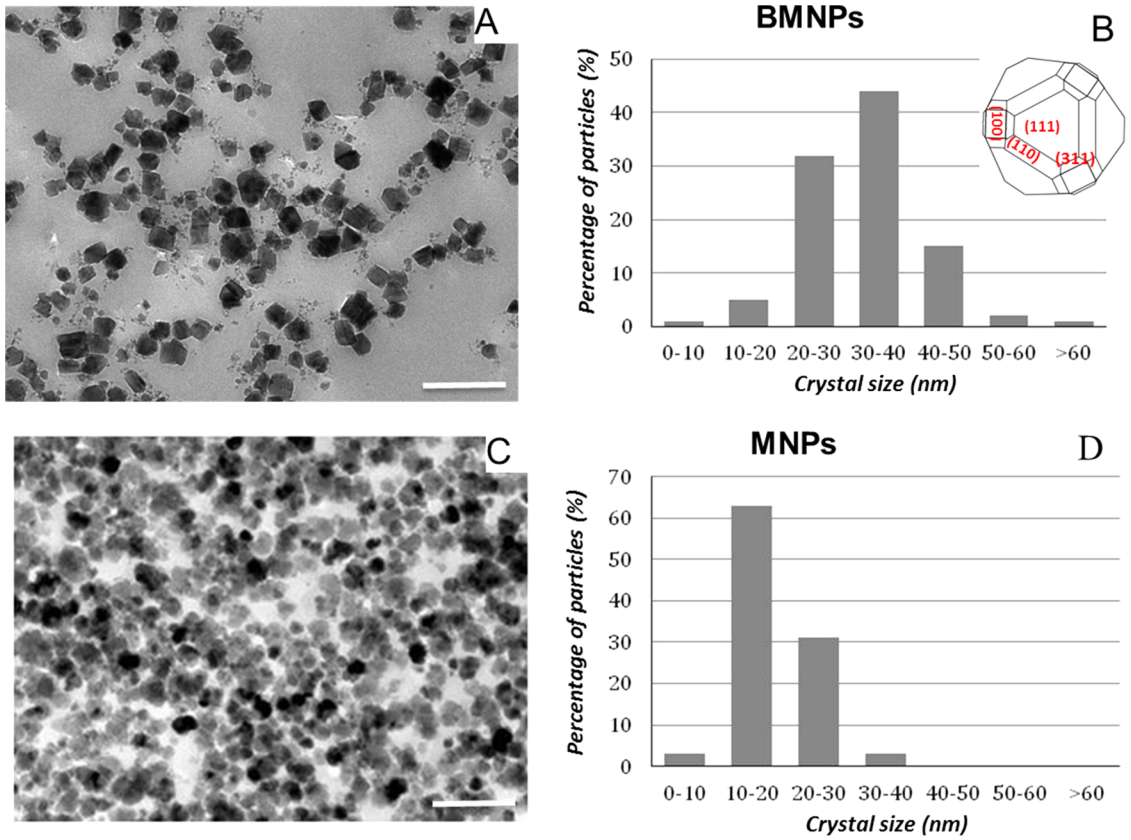

Figure 1. Magnetite crystals synthesized in the presence of MamC (10 μg/mL) (BMNPs): (A) TEM images, (B) crystal size distribution. Inset: modelization of BMNPs from HRTEM data by using SHAPE v7.3 Magnetite crystals synthesized in the absence of any protein (inorganic magnetite: MNPs): (C) TEM images, (D) crystal size distribution. Scale bars in Figure 1A and 1C is 100 nm.

Alternatively, the LF model considers that the adsorption energy is heterogeneous, and cooperativity effects are also taken into account. This model is described by eq 2, where K_{LF} is the LF affinity constant and r is the cooperativity coefficient. Values of $r > 1$ indicate a positive cooperativity, while values of $r < 1$ indicate a negative cooperativity.[31]

$$Q = \frac{Q_{max}(K_{LF}C_e)^r}{1 + (K_{LF}C_e)^r} \quad (2)$$

Since the concentration of DOXO in the equilibrium (C_e) is dependent on the error of $[DOXO]_{sn}$, that being associated with the error on the measurements of the absorbance, the calculations of the errors in C_e and Q_{max} were performed by applying the propagation error theory.

Drug release was analyzed at pH 7.4 and pH 5.0. The DOXO−BMNPs were suspended in HEPES (10 mM, 1 mL, pH 7.4) or acetate buffer (10 mM, 1 mL, pH 5.0), both solutions containing NaCl 0.2 M. Suspensions were incubated at 37 °C, 150 rpm for different time intervals up to 48 h. Samples were centrifuged at 10 000 rpm for 5 min, and supernatants were analyzed by UV−vis spectroscopy. The release efficiency (D_R) was defined by eq 3, as the ratio between the amount of released molecules at a fixed time t ($Q(t)$) and the Q_{max}.[20]

$$D_R = \frac{Q_{(t)}}{Q_{max}} \times 100 \quad (3)$$

Hemocompatibility Test. Hemocompatibility was assessed ex vivo, as previously described with some modifications.[32−34] Briefly, 0.5 mL of human blood was obtained by intravenous puncture from an informed volunteer and centrifuged (10 min, 2000 rpm). Supernatants were discarded, and the red blood cells (RBCs) were resuspended in phosphate buffered saline (PBS) and washed twice with PBS to remove traces of plasma. RBCs were then resuspended in PBS, at a concentration of 4×10^9 cells/mL. Serial dilutions (0.1−100 μg/mL) of the BMNPs-citrate (either treated under UV or autoclaved) were prepared and a volume of 0.5 mL of the specific dilution was mixed with 25 μL of RBC suspension. The mixtures were incubated at 25 °C under continuous agitation for 10 min or 24 h and then centrifuged (5 min, 2000 rpm). The absorbance of the solution was measured at 540 nm wavelength, and the values were compared with the positive (distilled water) and negative (PBS) controls. For blood smears preparation, after incubation of cells with BMNPs, the latter were withdrawn by a magnet, cells were washed once, and smears were prepared and stained using the May-Grünwald Giemsa (Biolyon, Dardilly, France) technique. Samples were analyzed by optical microscopy (Nikon ECLIPSE Ci), and photos were taken with a digital camera.

Cytotoxicity Tests of BMNPs and DOXO−BMNPs. The GTL-16 cell line, derived from a poorly differentiated human gastric carcinoma, was maintained in Dulbecco's modified Eagle's medium, supplemented with 10% fetal calf serum, 50 U/mL penicillin, and 50 μg of streptomycin. Cells were transplanted when they were at 80−90% confluency to 1/3−1/4. This cell line was used previously to test other nanoparticles as drug carriers because it is easily manageable and, moreover, it can be considered a tumor cell model as it overexpresses the tumor marker Met/hepatocyte growth factor receptor, which is targetable by a monoclonal antibody used as a probe.[35] The cytotoxicities of the nonloaded BMNPs or of the DOXO−BMNPs were evaluated on this cell line, as already described.[18,35] Approximately, 12×10^3 cells/well were incubated in 96-well plates for 24 h. Then, different equimolar amounts of DOXO, either soluble or adsorbed to the BMNPs (DOXO−BMNPs) as well as of nonloaded BMNPs-citrate, were added. After 3 days of incubation, cell viability was evaluated by the 3-(4,5-dimethylthiazol-2-yl)-2,5-diphenyltetrazolium bromide (MTT) colorimetric assay. Briefly, 20 μL of MTT solution (5 mg/mL in PBS solution)

DOI: 10.1021/acs.langmuir.8b03109
Langmuir 2018, 34, 13713−13724

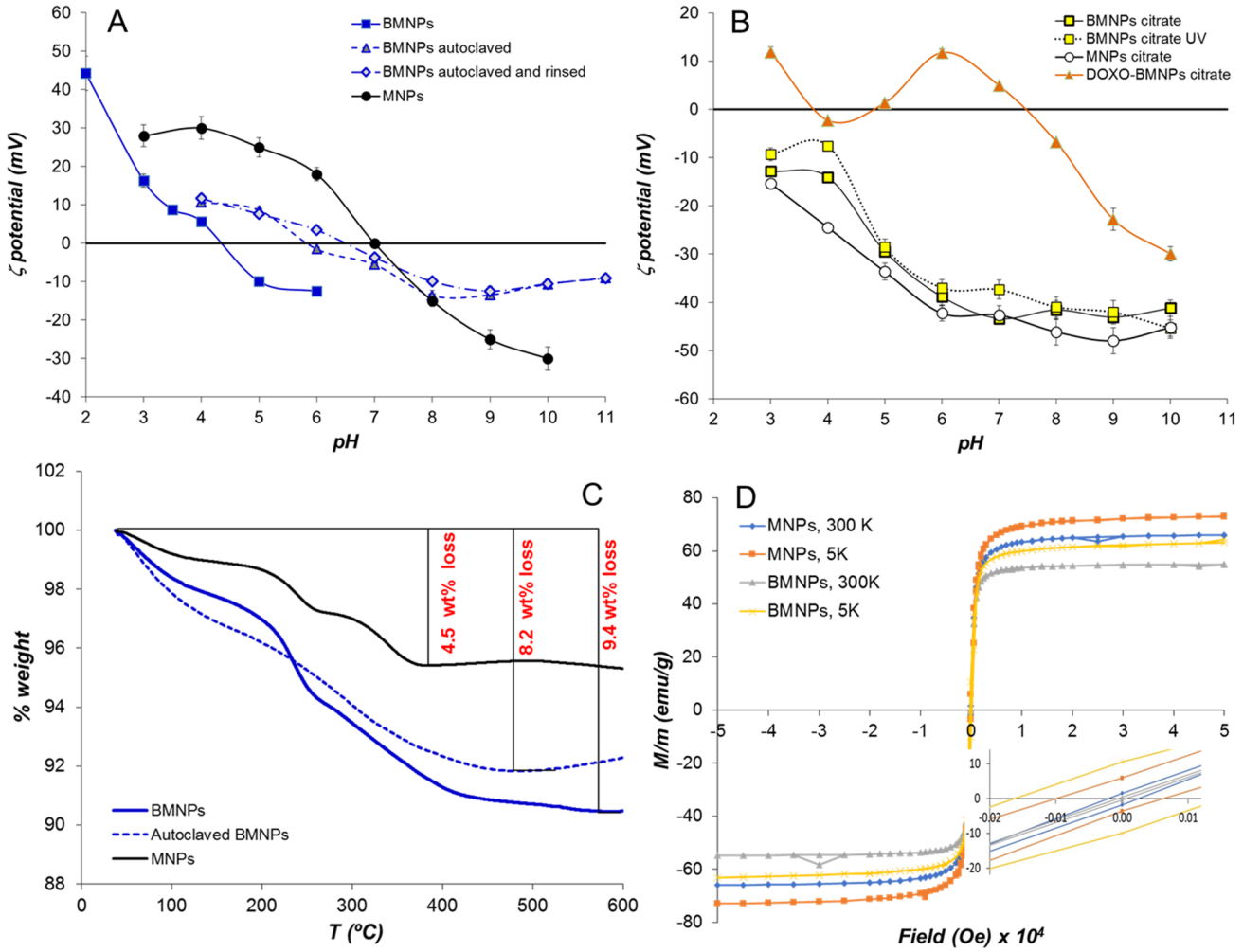

Figure 2. ζ-Potential of: (A) MNPs, BMNPs, autoclaved BMNPs, and autoclaved BMNPs and then rinsed with the goal of removing MamC. These particles were not coated with citrate; (B) MNPs, BMNPs, BMNPs treated with UV, and DOXO−BMNPs coated with citrate. (C) Thermogravimetric analyses of MNPs, BMNPs, and autoclaved BMNPs. (D) Hysteresis cycle of BMNPs and MNPs at 5 and 300 K. Inset: detail of the cycle in the absence of external magnetic field. In some data points, the error bar is smaller than the symbol.

was added to each well, and the plate was incubated at 37 °C for 2 h. Afterward, the supernatants were carefully aspirated, and 125 μL of 0.2 N HCl in isopropanol was added to dissolve the formazan crystals formed. Finally, the optical density was measured in a multiwell reader (2030 Multilabel Reader Victor TM X4, PerkinElmer) at 570 nm. Viability of parallel cultures of untreated cells was taken as 100% viability, and values obtained from treated cells were referred to this value. Experiments were performed three times using 3 replicates for each sample.

RESULTS AND DISCUSSION

XRD analyses (not shown) reveal that magnetite comprises 100% of the solid precipitated in the experiments. TEM micrographs (Figure 1) show that most BMNPs exhibited isometric crystals with well-developed faces and a size ranging from 20 to 50 nm, with an average crystal size of 33 ± 11 nm. Inorganic magnetites, in turn, display poorly defined morphologies and a crystal size ranging from 10 to 30 nm, with an average crystal size of 15 ± 6 nm (Figure 1).

The specific surface area (SSA) determined by BET is 97 ± 2 m^2/g. This value is higher than the geometric surface area determined for 40 nm size magnetite (density ∼5 g/cm^3), which is 30 m^2/g, and higher than the geometric surface area for particles displaying the octahedral morphology when considering the size distribution for BMNPs of Figure 1 (∼48 m^2/g). Several reasons can account for this difference between the calculated and measured SSA by the BET method. On the one hand, it is necessary to consider that these biomimetic nanoparticles are covered by MamC in such an amount that the surface charge of the magnetite is that of the protein, as it will be detailed later. Therefore, the attached MamC contributes to the SSA of the BMNPs. Also, surface roughness originated in surface-terminated crystals by spirals, terraces, or kinked zones is an important contribution to the SSA. On the other hand, the crystals tend to aggregate and pack forming mesoporous structures, especially the smaller particles. Specific surface area BET of mesoporous magnetite nanoparticles reported in the literature shows values as high as ∼90[36] and 286.9 m^2/g for 98 nm size Fe_3O_4 nanoparticles,[37] 53.7 m^2/g for ∼14 nm biogenic magnetite particles,[38] 172 m^2/g for 6.9 nm Fe_3O_4 nanoparticles,[39] and from 99 m^2/g (unmodified magnetite) to 400 m^2/g when increasing the SiO_2 content in SiO_2/Fe_3O_4 nanocomposites.[40] Therefore, our value of 97 m^2/g is within the range of SSA determined for magnetite in other studies.

The plots of ζ-potential versus pH (Figure 2) reveal significant differences among the values measured in aqueous

DOI: 10.1021/acs.langmuir.8b03109
Langmuir 2018, 34, 13713−13724

suspensions of either uncoated nanoparticles (Figure 2A) or coated with citrate (Figure 2B). Citrate-coated nanoparticles are negatively charged within the studied pH range, which is consistent with the exposure of the carboxylic groups present in the citrate. All MNPs (MNPs, BMNPs, BMNPs autoclaved, or BMNPs autoclaved and rinsed) that were not coated with citrate are positively charged at low pH values and negatively charged at high pH values. The isoelectric point (iep) for these particles, determined from the ζ-potential calculations, is 7.0 for MNPs, 4.4 for BMNPs, 5.8 for BMNPs autoclaved, and 6.5 for BMNPs autoclaved and rinsed. These findings suggest that MamC is strongly attached to (or maybe incorporated into) the crystals because even after a careful rinsing with the aim of removing the protein from the crystal, the surface charge of the biomimetic nanoparticles was never that of the pure inorganic magnetites. This observation is further confirmed by TGA analyses (Figure 2C). The total weight per cent (wt %) loss of BMNPs is 9.4, while that for MNPs is 4.5, indicating that BMNPs are composed of 95.1 wt % of magnetite and 4.9 wt % of MamC. The amount of MamC in the BMNPs autoclaved is slightly lower (3.7 wt %). Therefore, MamC seems to have an important role in controlling not only the nanoparticle size distribution but also their surface properties. These results are in agreement with the saturation magnetization (M_s) data (Figure 2D). As it can be seen in the inset, both MNPs and BMNPs present remanent magnetization at 5 K in the absence of an external field, but not at 300 K, which confirms that both particles are superparamagnetic and have a blocking temperature < 300 K. These data are in agreement with the blocking temperatures reported in Valverde-Tercedor.[15] These authors concluded that the magnetization measurements of BMNPs vs those of MNPs indicate that the first type of nanoparticles is larger and, thus, has a larger magnetic moment per particle. According to our data, M_s for BMNPs is 55 emu/g, while that for MNPs is 66 emu/g (Figure 2D). The difference in saturation magnetization between BMNPs and MNPs is not so high considering the dilution effect of the coating, and the reduction in the M_s value of the BMNPs could be caused by the incorporation of MamC. In fact, considering the TGA weight loss of BMNPs 9.4 and MNPs 4.5%, the corrected values of M_s for BMNPs and MNPs should be, respectively, $55/(1 - 0.094) = 61$ emu/g and $66/(1 - 0.045) = 69$ emu/g, which indicates that they are comparable.

The iep for BMNPs (4.4) is very close to that for MamC (iep 4.47),[15] which suggests that MamC attaches (at least, partially) to the magnetite surface during crystal growth and changes their surface properties with respect to those produced by inorganic synthesis in the absence of any protein, in which the iep observed is ~7. This is consistent with the interaction model between MamC and magnetite proposed by other authors[41,42] and with the isothermal titration calorimetry data obtained in a previous work[41] that showed a strong interaction between MamC and magnetite. According to the model proposed by these authors, the unique control exerted by MamC over the nucleation and growth process of magnetite is based on the confluence of two mechanisms. Firstly, and similar to other acidic proteins like Mms6,[8,12] MamC interacts with aqueous iron cations through an ionotropic effect, thus inducing magnetite nucleation in the negatively charged areas created by the concentration of acidic amino acids, which in MamC are present both in the loop between the two MamC transmembrane domains and in the C-terminal domain.[15,41,42] Secondly, MamC has the unique characteristic that it provides an extended surface for magnetite templated growth due to the fact that two negatively charged amino acids in this loop are at a distance that matches that between Fe cations in the specific crystal faces in magnetite (111), (110), (100), and (311).[42] This templated growth extensively changes the magnetite nucleation and growth process, resulting in crystals that are different from those produced inorganically. The protein sticks to these specific faces listed above, inhibiting or slowing down their growth, and thus these faces become mostly expressed in the final morphology of the MamC-mediated magnetite, as previously demonstrated.[42] A schematic image of the final morphology of BMNPs is shown in Figure 1B (inset). MamC is probably attached to these faces, and it is expected to cover, totally or partially, the surface of magnetite, providing such a crystal with new surface properties. This is particularly important when magnetite nanoparticles are intended as nanocarriers.

When the BMNPs are functionalized with DOXO and exposed to different pH values, the ζ-potential varies considerably within the studied pH range (Figure 2B). The binary biomimetic nanoparticles are positively charged at pH values < ~4 and from ~5 to ~7.5. At pH values above 7.5, the DOXO−BMNPs display negative ζ-potential values. This indicates that the binary biomimetic nanoparticles are not identical over the pH range, probably because once adsorbed on the BMNPs, different amounts of DOXO remain on the BMNPs depending upon the pH.

The time required to reach the equilibrium for DOXO adsorption (no net DOXO adsorption or desorption) was found to be 3 h (data not shown). This time is lower than the one required for citrate-coated apatite nanocrystals (10 h),[43] although it is higher than for citrate-coated gold nanoparticles (less than 30 s)[19] or graphene (less than 20 min).[20]

The amount of adsorbed drug per amount of nanoparticles (Q) from the adsorption isotherm (Figure 3) shows a nonlinear association with the amount of nonadsorbed DOXO (C_e), displaying an S-shaped curve with a drug loading capacity (Q_{max}) of 0.69 ± 0.03 mg DOXO/mg magnetite. This value, expressed in mg DOXO/mg adsorbent, is intermediate between those estimated for citrate-coated apatite (0.41[43]),

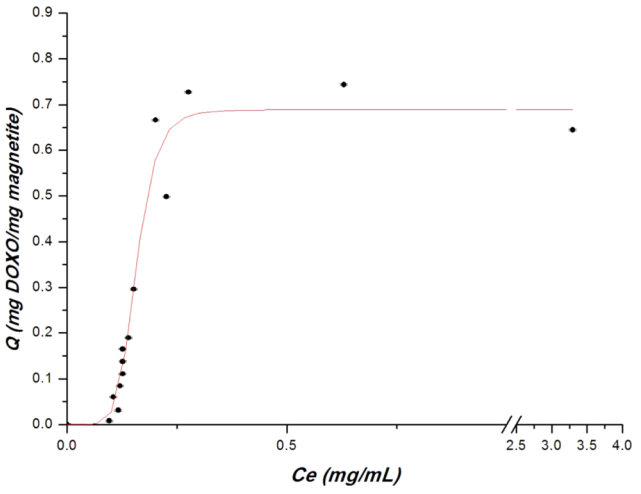

Figure 3. Adsorption isotherm of DOXO on BMNPs. The line represents the nonlineal weighted least-squares fitting of the experimental data according to the LF model. The vertical error bars are smaller than the symbol.

DOI: 10.1021/acs.langmuir.8b03109
Langmuir 2018, 34, 13713−13724

citrate-coated carbonated-apatite (0.44[43]), and superparamagnetic iron-doped apatite nanocrystals (0.45[43]) and that for graphene oxide nanoparticles (1.43[20]). However, if we normalize with respect to the specific surface area of our BMNPs (SSA = 97 ± 2 m^2/g) and those reported for these apatite samples (90, 93, and 44 m^2/g, respectively), the loading capacity is even lower.

The value of Q increases slowly initially, then rising exponentially and stabilizing thereafter. The experimental data were adjusted according to the Langmuir and Langmuir−Freundlich (LF) models. However, only the LF model, which introduces the effects of energetic heterogeneity of the surface and the cooperativity between DOXO molecules, fits the experimental data yielding an R^2 = 0.95901. The values of the LF affinity constant (K_{LF}) and cooperativity coefficient (r) parameters, calculated by means of this model (eq 2), were 6.33 ± 0.25 mL/mg magnetite and 6.97 ± 1.30, respectively. The parameter K_{LF} is in line with the one previously reported for iron-doped apatite nanocrystals[43] of 5.96 ± 3.27; however, the value of r is significantly higher than the 1.7 ± 0.4 reported for this adsorbent. Such a high r coefficient indicates a strong positive cooperativity between DOXO molecules during the adsorption process. Thus, these parameters reveal that adsorbed molecules are interacting not only with the substrate but also between themselves as a pathway to decrease the adsorption energy.

The DOXO release at physiological pH (pH 7.4) is practically negligible, with release efficiency (D_R) (eq 3) values at 24 h that do not exceed 5% of the initially adsorbed DOXO (Figure 4). However, the release at pH 5 is quite fast at

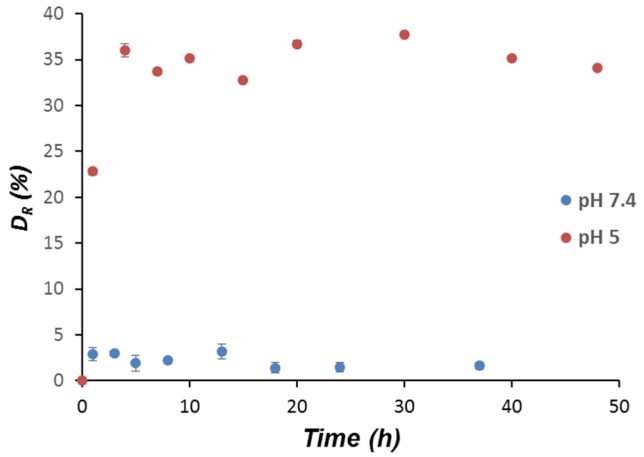

Figure 4. Kinetics of DOXO release from loaded DOXO−BMNPs over time at physiological pH (pH 7.4) and at acidic pH (pH 5) at 25 °C.

the beginning since it only takes 1 h to release 20% of the initially adsorbed DOXO. Then, the desorption rate decreases slowly up to a maximum of ∼35% of the initially adsorbed DOXO, which is achieved in the next 9−10 h. This sustained and long-lasting release in time of the chemotherapeutic drug after the first burst is beneficial in view of the expected nanomedical applications of these BMNPs.

ζ-Potential values shown in Figure 2A,B are key to understand the mechanisms involved in DOXO adsorption to and desorption from MamC-mediated biomimetic magnetite nanoparticles. In the purely inorganic MNPs, for instance, the hydrated surfaces remain basically uncharged at physiological pH (Figure 2) as a consequence of the dominant neutral surface species ≡Fe(II,III)OH at this pH (eq 4)[44]

$$\equiv \mathrm{Fe(II,\,III)OH_2^+} - \mathrm{H^+} \rightarrow \equiv \mathrm{Fe(II,\,III)OH} - \mathrm{H^+} \rightarrow \equiv \mathrm{Fe(II,\,III)O^-}\ \mathrm{pH_{iep}} \sim 7 \quad (4)$$

According to the equilibrium of the Fe-bearing species present on the surface of magnetites in aqueous solutions, at acidic pH, the magnetite surface is positively charged, as the dominant species are $Fe(II,III)OH_2^+$. As the pH value increases, Fe(II,III)OH becomes dominant, and, at even higher pH values, the dominant species are $Fe(II,III)O^-$, in these conditions the surface of magnetite being negatively charged. Since the iep of magnetite is ∼7, the MNPs are neutral at physiological pH (Figure 2A), and, therefore, the functionalization of these MNPs could be attained only by means of providing new functional groups, that is, covering with citrate or other acids, which are able to change the ζ-potential (and thus, the iep) of magnetite in aqueous solution[45] or by linking the molecule to the MNP surface by either covalent or hydrogen bond, which would make it difficult to release the coupled molecule at the desired site.

By contrast, BMNPs display an iep of 4.4, and since ζ-potential and TGA analyses show that MamC is attached to the BMNPs, the changes in the ζ-potential values of BMNPs with respect to those of MNPs should be attributed to the presence of MamC. Both the MamC loop and C-terminal display iep values of 4.31 and 4.25, respectively (calculated by using Expasy ProtParam tool). Therefore, it seems plausible to hypothesize that both protein domains are exposed at the surface of the BMNPs. In fact, some authors[35,41] demonstrated that the MamC loop attaches to the magnetite surface and that MamC forms mainly monomers and dimers in solution, probably through the hydrophobic (transmembrane) domains. According to these observations, it could be hypothesized that both a mixture of populations of monomers as well as dimers are attached to the magnetite surface, mainly through the loop, thus exposing the C-terminal (monomers) and the MamC loop of the attached dimer to the outer layer. Therefore, the iep of the BMNPs becomes that of the exposed domains, that is, MamC loop (4.31) and C-terminal (4.26). The iep of these domains is determined by the predominant negatively charged amino acids [acidic amino acids (Asp and Glu), and the lower number of positively charged amino acids (Lys and Arg)] present in these regions. In particular, the MamC loop (32 amino acids) contains 5 acidic and 2 basic amino acids. Similarly, the C-terminal of MamC (43 amino acids) contains 10 acidic and 3 basic amino acids. The pK_a corresponding to the carboxylic group (−COOH) of the acidic amino acids is 3.86 for the Asp and 4.25 for the Glu, while that corresponding to the amino group ($-NH_2$) of the basic amino acids is 10.79 for Lys and 12.48 for Arg. At physiological pH, the number of functional groups in the negative form ($-COO^-$) is higher than that of the groups in the positive form ($-NH_3^+$) and, therefore, the BMNPs display a negative ζ-potential value. This is important since it allows the functionalization of the BMNPs with molecules that display positively charged functional groups at these pH values by simple electrostatic interactions.

In this context, within the concentration ranges used in this work, DOXO forms dimers with antiparallel conformation in which their amino groups are directed to opposite directions.[46] Most of these amino groups with a pK_a 8.2[18] are protonated ($-NH_3^+$) at pH 7.4, thus leading the DOXO dimers to display

DOI: 10.1021/acs.langmuir.8b03109
Langmuir 2018, 34, 13713−13724

a net positive charge. Since, at the same pH, BMNPs display a net negative charge, the DOXO adsorption on BMNPs will be driven by electrostatic interactions between the protein acidic amino acids located either at the C-terminal or at the loop. In the MamC-free magnetite faces (which are a minority), the DOXO adsorption could potentially also take place, but most probably through a covalent bond, forming esters, or by hydrogen bond. The pH-responsive release of DOXO molecules from these faces will hardly occur.

Since distinct magnetite crystal faces with different ionic configurations (and, thus, different net surface charges) are expressed in the final morphology of BMNPs (Figure 1A, B (detail)), different concentrations of MamC and distinct electrostatic interactions between the particle and DOXO are expected along the surface of the nanoparticle, resulting in a nonhomogenous DOXO distribution along the crystal surface. In fact, the adsorption isotherm and its fitting to the Langmuir–Freundlich model strongly suggest that the surface of the magnetite is not energetically homogeneous.

On the other hand, electrostatic interactions may not be the only ones involved, as suggested by the r value of the Langmuir–Freundlich model, which indicates a positive cooperativity between the DOXO molecules during their adsorption. This phenomenon results in the reduction of the adsorption energy of nonoccupied sites surrounded by occupied sites, also in accordance with the S-shape of the adsorption isotherm. By consequence, the adsorption of DOXO molecules favors the adsorption of more DOXO molecules until the Q_{max} is reached. This model of electrostatic interactions and even the positive cooperative effect were also found in DOXO adsorption on citrate-coated apatite nanocrystals.[18]

DOXO release at physiological pH 7.4 was practically negligible (D_R < 5%), while this release exceeded 35% at pH 5, the pH mimicking the conditions in the endosome–lysosome compartment[47] (Figure 4). On the basis of the electrostatic interaction model, we propose that when the pH value of the microenvironment decreases and approximates the pH value at which the particle reaches its iep, the electrostatic interaction between DOXO and the $-COO^-$ weakens and the electrostatic repulsions between adsorbed adjacent DOXO molecules become stronger. As a result, DOXO is desorbed from the nanoparticle surface, starting from the outer layers of adsorbed molecules, which are probably those with the weakest electrostatic bonds. The calculated value of 35% of drug release at pH 5 is comparable to that obtained by other authors using iron oxide nanoparticles at pH 4.5.[45] However, the stability of DOXO–BMNPs at pH 7.4 (maximum release of 5%) is greater than that of the iron oxide nanoparticles described above[45] (~17% release in just 1 h). This is important for clinical practice in which no release of drug should occur in the blood stream until the target site is reached.

The cytocompatibility of nonloaded BMNPs-citrate was analyzed by measuring the survival of GTL-16 cells incubated for 3 days with different concentrations of nanoparticles in an MTT assay. They were found to be not significantly cytotoxic since they induced a reduction in cell viability of only 15% at the highest concentration used (Figure 5). Similar cytocompatibility was observed also on other cell lines, such as the murine 3T3-NIH, m17.ASC, and the human Huh7 hepatocellular carcinoma cells (data not shown). By contrast, when the same amounts of BMNPs uploaded with DOXO were

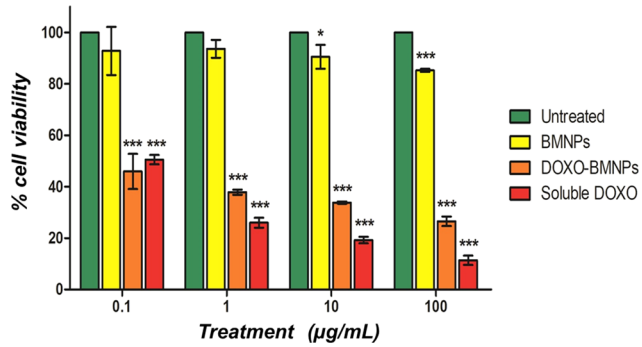

Figure 5. Cytocompatibility of the nonloaded BMNPs and cytotoxic activity of the DOXO–BMNPs on GTL-16 cell line. Cells were incubated with the same amounts of DOXO, either soluble or bound to MNPs and with comparable amounts of nonloaded BMNPs for 72 h, and then cell viability was evaluated in an MTT assay. DOXO–BMNPs ratio was 0.70/1 mg. Untreated cells were taken as reference value (100%) of viability. Analysis of variance one-way reveals statistical significance referred to untreated cells ($*p \leq 0.05$; $***p \leq 0.001$). Data are the average ± standard error of the average (SEM) of three experiments performed in triplicates.

tested in this assay, they reduced cell survival in a dose-dependent manner up to more than 70% at the highest dose tested of 100 μg/mL of DOXO. In the same experiments, soluble DOXO was found to be more toxic than BMNPs-uploaded DOXO. Similar data have already been reported for other types of NPs, such as hydroxyapatite NPs,[35] and can be accounted for by the fact that in this condition DOXO could be internalized at a lower rate. Therefore, another further important property of the BMNPs described herein is their good cytocompatibility when incubated *in vitro* with a human gastric carcinoma cell line, but at the same time the possibility of becoming an efficient carrier for therapeutic molecules such as DOXO, which was shown to be able to kill these cells.

Since drug-loaded nanocarriers are generally administered by intravenous injection, their hemocompatibility was assessed by incubating them with red blood cell suspensions. BMNPs-citrate, either untreated or sterilized either under UV or by autoclave, were all found to be nontoxic in a wide concentration range in the hemolytic *ex vivo* test. Indeed, only at the highest dose tested of 100 μg/mL could they induce the release of about 28% of hemoglobin in the case of UV-treated BMNPs and of an insignificant 2% of hemoglobin in the case of autoclaved BMNPs (Figure 6A,B). Hemocompatibility was tested also by performing smear experiments on two series of whole blood samples, incubated with BMNPs-citrate, either untreated (Figure 6C) or incubated with two concentrations (10 and 100 μg/mL) of BMNPs sterilized either under UV (Figure 6D,F) or by autoclave (Figure 6E,G). In all these cases, cells did not display signs of suffering or aggregation. We can thus conclude that BMNPs-citrate are hemocompatible since they caused only a slight but acceptable RBC damage and only at the highest concentrations. No other significant differences in cytocompatibility or ξ-potential were observed because of the treatments with UV.

Hydrodynamic radius measurements show that there are different populations with different hydrodynamic sizes. Most of the nanoparticles are aggregated with a size > 1000 nm (Figure 7) and, therefore, they could not undergo EPR effect. However, there is still a population with a size ≤150 nm (dots within the colored area in the figure) that could reach the

DOI: 10.1021/acs.langmuir.8b03109
Langmuir 2018, 34, 13713–13724

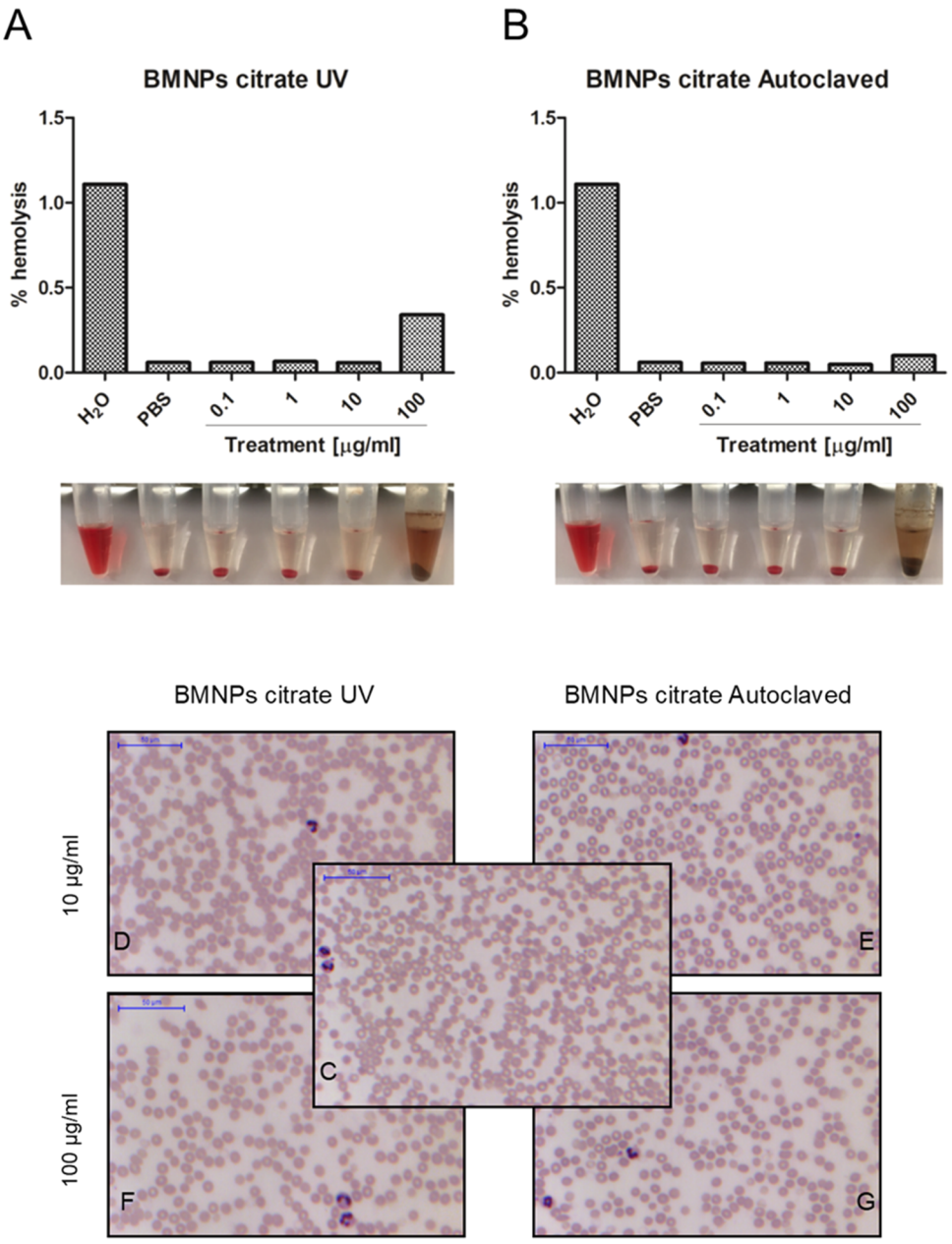

Figure 6. Hemolytic response of human red blood cells (RBCs) incubated with serial dilutions of BMNPs, sterilized by UV (A) or by autoclave (B), PBS, or distilled water for 24 h at room temperature. Top panels, percentage of hemolysis in comparison with the positive (distilled water) and negative (PBS) controls, assessed by the absorbance of supernatant at 540 nm wavelength. Results are shown as means ± standard error of the mean (SEM). Bottom panels, representative images of RBC mixtures with PBS, BMNP serial dilutions, and distilled water after 24 h of incubation followed by centrifugation. Results in line with were observed also with untreated BMNPs. Pictures of the blood smears prepared from ethylenediamine tetraacetic acid-anticoagulated blood incubated in PBS (C), with BMNPs, sterilized by UV (D, F) or by autoclave (E, G), 10 μg/mL (D, E), or 100 μg/mL. Scale bars in Figures is 50 μm.

tumor site by EPR effect.[48] Nevertheless, EPR effect by itself might not be enough in this case to ensure a correct targeting of the tumor site, and other ways of cell targeting such as additional coupling of the BMNPs with monoclonal antibodies combined with active guidance of the BMNPs to the target site by means of the application of an external magnetic field should be explored in the future to increase the efficiency of the targeting.

The slowest sedimentation occurred in the samples containing nonloaded BMNPs (0.0192 mm/s), and the fastest sedimentation occurred in DOXO−BMNPs, 0.038 mm/s. These results are in accordance with the data of hydrodynamic radius, in which it was observed that the latter binary biomimetic nanoparticles exhibited the highest percentage of aggregates. Colloidal stability of these binary nanoparticles, nevertheless, should be improved in the future.

As a summary, there are a number of findings that make BMNPs unique and good candidates as potential drug nanocarriers for targeted drug delivery, although colloidal stability still needs to be improved. The advantages of the biomimetic nanoparticles of the present study are: (1) nonloaded BMNPs are cytocompatible, but they become cytotoxic when coupled with DOXO; (2) they exhibit a large magnetic moment per particle; (3) DOXO adsorption and

DOI: 10.1021/acs.langmuir.8b03109
Langmuir 2018, 34, 13713−13724

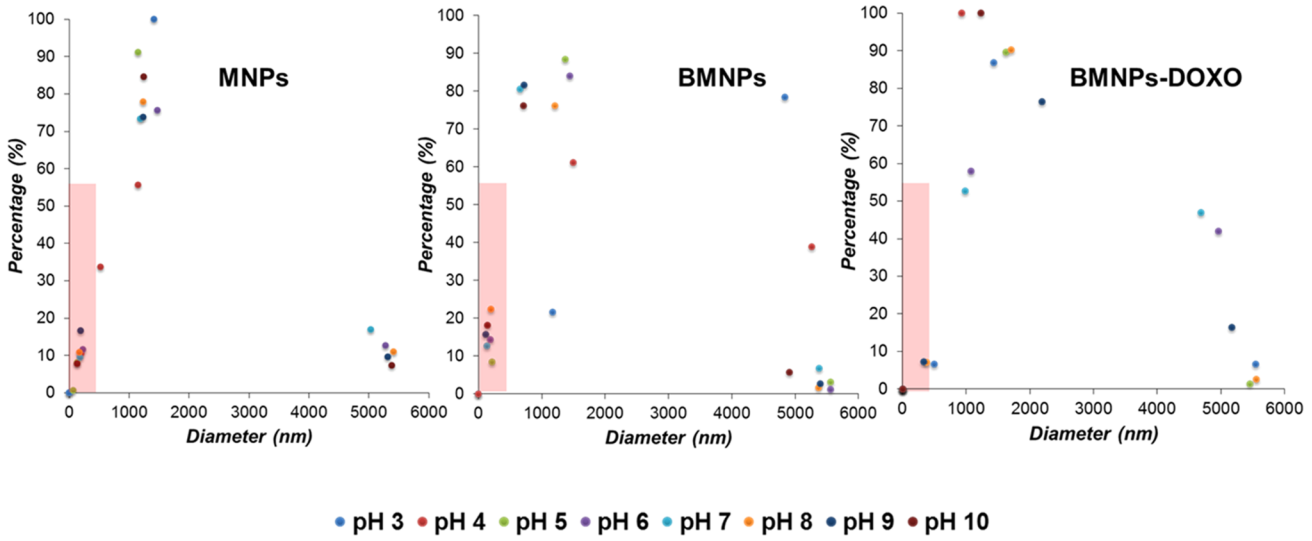

Figure 7. Hydrodynamic size of the inorganic magnetic nanoparticles (MNP), biomimetic magnetic nanoparticles (BMNPs), and DOXO−BMNPs. The percentage of nanoparticles of a certain size for the different pH values measured is plotted. Colored area marks the size range of hydrodynamic radius ≤ 150 nm.

release can be controlled efficiently by changes in pH, like those that naturally occur when entering from the blood stream to the tumor tissues; (4) MamC provides the surface of the BMNPs with functional groups that allow coupling with other molecules; and (5) the DOXO−BMNPs nanoassembly is quite stable at physiological pH values.

CONCLUSIONS

The potential role of BMNPs produced in the presence of MamC as drug nanocarriers has been assessed for the first time. The BMNPs produced in the present study are pH-sensitive nanocarriers in which DOXO adsorption is mostly driven by electrostatic interactions between positively charged DOXO amino groups and negatively charged acidic residues of the MamC that is attached to the surface of the crystal. By contrast, desorption of DOXO from the DOXO−BMNPs nanoassembly is achieved by weakening this bond as pH decreases and approaches the iep of the BMNPs (iep 4.4). The adsorption process follows a Langmuir−Freundlich model, which shows that the surface of the magnetite is energetically heterogeneous and displays positive cooperativity. The BMNPs coupled with DOXO (DOXO−BMNPs) are stable at physiological pH with maximum releases of 5% of the initial DOXO adsorbed, while the desorption process is efficient since about 35% of the adsorbed drug was released in just 4 h at pH 5. Moreover, these DOXO−BMNPs nanoassemblies are cytotoxic for the GTL-16 carcinoma cell line, in which they induced more than 70% mortality. This toxicity was dependent on the DOXO adsorbed to the BMNPs since nonfunctionalized nanoparticles were highly cytocompatible and hemocompatible when in the presence of red blood cells. All together, these data indicate that BMNPs are unique magnetite nanoparticles with novel properties acquired thanks to their interaction with the protein MamC and, therefore, their potential as nanocarriers should be further explored in future studies.

AUTHOR INFORMATION

Corresponding Author

*E-mail: cjl@ugr.es. Phone: (+34) 958 249833.

ORCID

Concepcion Jimenez-Lopez: 0000-0002-5645-2079

Notes

The authors declare no competing financial interest.

ACKNOWLEDGMENTS

Thanks go to Ma Antonia Fernandez Vivas and Rafael Lopez-Moreno for technical assistance in the laboratory and data analysis, Angel Delgado Mora for assistance in electrophoretic mobility measurements, and to the CIC personnel of the University of Granada for technical assistance in the TEM. Thanks go to Nicolás López Baeza for some of the electrophoretic mobility measurements. C.J.-L. wants to thank projects CGL2013-46612 and CGL2016-76723 from the Ministerio de Economía y Competitividad from SPAIN and Fondo Europeo de Desarrollo Regional (FEDER) for financial support and Unidad Científica de Excelencia UCE-PP2016-05 of the University of Granada. This research is original and had a financial support also from the Università del Piemonte Orientale "A. Avogadro", Italy. We also wish to thank the Senior Editor of the Journal, Dr Zhan Chen, and three anonymous reviewers for their suggestions that greatly improved the present manuscript.

REFERENCES

(1) Alphandéry, E.; Faure, S.; Raison, L.; Duguet, E.; Howse, P. A.; Bazylinski, D. A. Heat production by bacterial magnetosomes exposed to an oscillating magnetic field. *J. Phys. Chem. C* **2011**, *115*, 18−22.

(2) Prozorov, T.; Bazylinski, D. A.; Mallapragada, S. K.; Prozorov, R. Novel magnetic nanomaterials inspired by magnetotactic bacteria: Topical review. *Mater. Sci. Eng. R* **2013**, *74*, 133−172.

(3) Mou, X.; Ali, Z.; Li, S.; He, N. Applications of magnetic nanoparticles in targeted drug delivery system. *J. Nanosci. Nanotechnol.* **2015**, *15*, 54−62.

(4) Estelrich, J.; Escribano, E.; Queralt, J.; Busquets, M. A. Iron oxide nanoparticles for magnetically-guided and magnetically-responsive drug delivery. *Int. J. Mol. Sci.* **2015**, *16*, 8070−8101.

(5) Doane, T. L.; Burda, C. The unique role of nanoparticles in nanomedicine: imaging, drug delivery and therapy. *Chem. Soc. Rev.* **2012**, *41*, 2885−2911.

DOI: 10.1021/acs.langmuir.8b03109
Langmuir 2018, 34, 13713−13724

(6) Bazylinski, D. A.; Frankel, R. B. Magnetosome formation in prokaryotes. *Nat. Rev. Microbiol.* **2004**, *2*, 217−230.
(7) Sun, J.; Tang, T.; Duan, J.; Xu, P.-X.; Wang, Z.; Zhang, Y.; Wu, L.; Li, Y. Biocompatibility of Bacterial Magnetosomes: Acute Toxicity, Immunotoxicity and Cytotoxicity. *Nanotoxicology* **2010**, *4*, 271−283.
(8) Amemiya, Y.; Arakaki, A.; Staniland, S. S.; Tanaka, T.; Matsunaga, T. Controlled formation of magnetite crystal by partial oxidation of ferrous hydroxide in the presence of recombinant magnetotactic bacterial protein Mms6. *Biomaterials* **2007**, *28*, 5381−5389.
(9) Kolhatkar, A. G.; Jamison, A. C.; Litvinov, D.; Willson, R. C.; Lee, T. R. Tuning the Magnetic Properties of Nanoparticles. *Int. J. Mol. Sci.* **2013**, *14*, 15977−16009.
(10) Zhang, F.; Zhao, L.; Wang, S.; Yang, J.; Lu, G.; Luo, N.; Gao, X.; Ma, G.; Xie, H. Y.; Wei, W. Construction of a biomimetic magnetosome and its application as a siRNA carrier for high-performance anticancer therapy. *Adv. Funct. Mater.* **2017**, *28*, No. 1703326.
(11) Timko, M.; Dzarova, A.; Kovac, J.; Skumiel, A.; Jozefczak, A.; Hornowski, T.; Gojzewski, H.; Zavisova, V.; Koneracka, M.; Sprincova, A.; Strbak, O.; Kopcansky, P.; Tomasovicova, N. Magnetic properties and heating effect in bacterial magnetic nanoparticles. *J. Magn. Magn. Mater.* **2009**, *321*, 1521−1524.
(12) Boucher, M.; Geffroy, F.; Prévéral, S.; Bellanger, L.; Selingue, E.; Adryanczyk-Perrier, G.; Péan, M.; Lefèvre, C. T.; Pignol, D.; Ginet, N.; Mériaux, S. Genetically tailored magnetosomes used as MRI probe for molecular imaging of brain tumor. *Biomaterials* **2017**, *121*, 167−178.
(13) Prozorov, T.; Mallapragada, S. K.; Narasimhan, B.; Wang, L.; Palo, P.; Nilsen-Hamilton, M.; Williams, T. J.; Bazylinski, D. A.; Prozorov, R.; Canfield, P. C. Protein-mediated synthesis of uniform superparamagnetic magnetite nanocrystals. *Adv. Funct. Mater.* **2007**, *17*, 951−957.
(14) Arakaki, A.; Webb, J.; Matsunaga, T. A novel protein tightly bound to bacterial magnetic particles in *Magnetospirillum magneticum* strain AMB-1. *J. Biol. Chem.* **2003**, *278*, 8745−8750.
(15) Valverde-Tercedor, C.; Montalbán-López, M.; Perez-Gonzalez, T.; Sanchez-Quesada, M. S.; Prozorov, T.; Pineda-Molina, E.; Fernandez-Vivas, M. A.; Rodriguez-Navarro, A. B.; Trubitsyn, D.; Bazylinski, D. A.; Jimenez-Lopez, C. Size control of in vitro synthesized magnetite crystals by the MamC protein of *Magnetococcus marinus* strain MC-1. *Appl. Microbiol. Biotechnol.* **2015**, *99*, 5109−5121.
(16) Bellocq, A.; Suberville, S.; Philippe, C.; Bertrand, F.; Perez, J.; Fouqueray, B.; Cherqui, G.; Baud, L. Low environmental pH is responsible for the induction of nitric-oxide synthase in macrophages. Evidence for involvement of nuclear factor-kappaB activation. *J. Biol. Chem.* **1998**, *273*, 5086−5092.
(17) Guo, M.; Yan, Y.; Zhang, H.; Yan, H.; Cao, Y.; Liu, K.; Wan, S.; Huang, J.; Yue, W. Magnetic and pH-responsive nanocarriers with multilayer core−shell architecture for anticancer drug delivery. *J. Mater. Chem.* **2008**, *18*, 5104−5112.
(18) Rodríguez-Ruiz, I.; Delgado-López, J. M.; Durán-Olivencia, M. A.; Lafisco, M.; Tampieri, A.; Colangelo, D.; Prat, M.; Gómez-Morales, J. pH-responsive delivery of doxorubicin from citrate-apatite nanocrystals with tailored carbonate content. *Langmuir* **2013**, *29*, 8213−8221.
(19) Curry, D.; Cameron, A.; MacDonald, B.; Nganou, C.; Scheller, H.; Marsh, J.; Beale, S.; Lu, M.; Shan, Z.; Kaliaperumal, R.; Xu, H.; Servos, M.; Bennett, C.; MacQuarrie, S.; Oakes, K. D.; Mkandawire, M.; Zhang, X. Adsorption of doxorubicin on citrate-capped gold nanoparticles: insights into engineering potent chemotherapeutic delivery systems. *Nanoscale* **2015**, *7*, 19611−19619.
(20) Wu, S.; Zhao, X.; Li, Y.; Du, Q.; Sun, J.; Wang, Y.; Wang, X.; Xia, Y.; Wang, Z.; Xia, L. Adsorption properties of doxorubicin hydrochloride onto graphene oxide: equilibrium, kinetic and thermodynamic studies. *Materials* **2013**, *6*, 2026−2042.
(21) Beretta, G. L.; Zunino, F. Molecular mechanisms of anthracycline activity. *Top. Curr. Chem.* **2008**, *283*, 1−19.
(22) Thorn, C. F.; Oshiro, C.; Marsh, S.; Hernandez-Boussard, T.; McLeod, H.; Klein, T. E.; Altman, R. B. Doxorubicin pathways: pharmacodynamics and adverse effects. *Pharmacogenet. Genomics* **2011**, *21*, 440−446.
(23) Kremer, L. C. M.; van Dalen, E. C.; Offringa, M.; Voûte, P. A. Frequency and risk factors of anthracycline-induced clinical heart failure in children: a systematic review. *Ann. Oncol.* **2002**, *13*, 503−512.
(24) Longhi, A.; Ferrari, S.; Bacci, G.; Specchia, S. Long-term follow-up of patients with doxorubicin-induced cardiac toxicity after chemotherapy for osteosarcoma. *Anticancer Drugs* **2007**, *18*, 737−744.
(25) Martin-Ramos, J. D. *Using XPowder: A Software Package for Powder X-ray Diffraction Analysis*, D.L. GR 1001/04, 2004.
(26) Von Smoluchowski, M. In *Handbuch der Elektrizitt und des Magnetismus*; Greatz, L., Ed.; J.A. Barth: Leipzig, Germany, 1921; Vol. *2*, p 366.
(27) Brunauer, S. P.; Emmett, H.; Teller, E. Adsorption of gases in multimolecular layers. *J. Am. Chem. Soc.* **1938**, *60*, 309−319.
(28) Beijnen, J. H.; et al. Aspects of the degradation kinetics of doxorubicin in aqueous solution. *Int. J. Pharm.* **1986**, *32*, 123−131.
(29) Langmuir, I. The adsorption of gases on plane surfaces of glass, mica and platinum. *J. Am. Chem. Soc.* **1918**, *40*, 1361−1403.
(30) Rill, C.; Kolar, Z. I.; Kickelbick, G.; Wolterbeek, H. T.; Peters, J. A. Kinetics and thermodynamics of adsorption on hydroxyapatite of the [160Tb]terbium complexes of the bone-targeting ligands DOTP and BPPED. *Langmuir* **2009**, *25*, 2294−2301.
(31) Turiel, E.; Perez-Conde, C.; Martin-Esteban, A. Assessment of the cross-reactivity and binding sites characterization of a propazine-imprinted polymer using the Langmuir-Freundlich isotherm. *Analyst* **2003**, *128*, 137−141.
(32) Fornaguera, C.; Calderó, G.; Mitjans, M.; Vinardell, M. P.; Solans, C.; Vauthier, C. Interactions of PLGA nanoparticles with blood components: protein adsorption, coagulation, activation of the complement system and hemolysis studies. *Nanoscale* **2015**, *7*, 6045−6058.
(33) Tombácz, E.; Farkas, K.; Foldesi, I.; Szekeres, M.; Illés, E.; Tóth, I. Y.; Nesztor, D.; Szabó, T. Polyelectrolyte coating on superparamagnetic iron oxide nanoparticles as interface between magnetic core and biorelevant media. *Interface Focus* **2016**, *6*, No. 20160068.
(34) Szekeres, M.; Tóth, I.; Illés, E.; Hajdú, A.; Zupkó, I.; Farkas, K.; Oszlánczi, G.; Tiszlavicz, L.; Tombácz, E. Chemical and colloidal stability of carboxylated core-shell magnetite nanoparticles designed for biomedical applications. *Int. J. Mol. Sci.* **2013**, *14*, 14550−14574.
(35) Iafisco, M.; Delgado-Lopez, J. M.; Varoni, E. M.; Tampieri, A.; Rimondini, L.; Gomez-Morales, J.; Prat, M. Cell surface receptor targeted biomimetic apatite nanocrystals for cancer therapy. *Small* **2013**, *9*, 3834−3844.
(36) Jain, S.; Shah, J.; Dhakate, S. R.; Gupta, G.; Sharma, C.; Kotnala, R. K. Environment-friendly mesoporous magnetite nanoparticles-based hydroelectric cell. *J. Phys. Chem. C* **2018**, *122*, 5908−5916.
(37) Ma, J.; Wang, L.; Wu, Y.; Dong, X.; Ma, Q.; Qiao, C.; Zhang, Q.; Zhang, J. Facile synthesis of Fe_3O_4 nanoparticles with a high specific surface area. *Mater. Trans.* **2014**, *55*, 1900−1902.
(38) Sundman, A.; Byrne, J. M.; Bauer, I.; Menguy, N.; Kappler, A. Interactions between magnetite and humic substances: redox reactions and dissolution processes. *Geochem. Trans.* **2017**, *18*, No. 6.
(39) Sarno, M.; Ponticorvo, E.; Cirillo, C. High surface area monodispersed Fe_3O_4 nanoparticles alone and on physical exfoliated graphite for improved supercapacitors. *J. Phys. Chem. Solids* **2016**, *99*, 138−147.
(40) Semko, L. S.; Khutornoi, S. V.; Abramov, N. V.; Gorbik, P. P. Synthesis, structure, and properties of large surface area Fe_3O_4/SiO_2 Nanocomposites. *Inorg. Mater.* **2012**, *48*, 374−381.
(41) Nudelman, H.; Valverde-Tercedor, C.; Kolusheva, S.; Perez Gonzalez, T.; Widdrat, M.; Grimberg, N.; Levi, H.; Nelkenbaum, O.; Davidov, G.; Faivre, D.; Jimenez-Lopez, C.; Zarivach, R. Structure-

DOI: 10.1021/acs.langmuir.8b03109
Langmuir 2018, 34, 13713−13724

function studies of the magnetite-biomineralizing magnetosome-associated protein MamC. *J. Struct. Biol.* **2016**, *194*, 244−252.
(42) Lopez-Moreno, R.; Fernández-Vivas, A.; Valverde-Tercedor, C.; Azuaga Fortes, A. I.; Casares Atienza, S.; Rodriguez-Navarro, A. B.; Zarivach, R.; Jimenez-Lopez, C. Magnetite nanoparticles biomineralization in the presence of the magnetosome membrane protein MamC: Effect of protein aggregation and protein structure on magnetite formation. *Cryst. Growth Des.* **2017**, *17*, 1620−1629.
(43) Iafisco, M.; Drouet, C.; Adamiano, A.; Pascaud, P.; Montesi, M.; Panseri, S.; Sarda, S.; Tampieri, A. Superparamagnetic iron-doped nanocrystalline apatite as a delivery system for doxorubicin. *J. Mater. Chem. B* **2016**, *4*, 57−70.
(44) Sun, Z. X.; Su, F. W.; Forsling, W.; Samskog, P. O. Surface Characteristics of Magnetite in Aqueous Suspension. *J. Colloid Interface Sci.* **1998**, *197*, 151−159.
(45) Kievit, F. M.; Wang, F. Y.; Fang, C.; Mok, H.; Wang, K.; Silber, J. R.; Ellenbogen, R. G.; Zhang, M. Doxorubicin loaded iron oxide nanoparticles overcome multidrug resistance in cancer in vitro. *J. Controlled Release* **2011**, *152*, 76−83.
(46) Agrawal, P.; Barthwal, S. K.; Barthwal, R. Studies on self-aggregation of anthracycline drugs by restrained molecular dynamics approach using nuclear magnetic resonance spectroscopy supported by absorption, fluorescence, diffusion ordered spectroscopy and mass spectrometry. *Eur. J. Med. Chem.* **2009**, *44*, 1437−1451.
(47) Geisow, M. J.; Evans, W. H. pH in the endosome. Measurements during pinocytosis and receptor-mediated endocytosis. *Exp. Cell Res.* **1984**, *150*, 36−46.
(48) Maeda, H. The enhanced permeability and retention (EPR) effect in tumor vasculature: the key role of tumor-selective macromolecular drug targeting. *Adv. Enzyme Regul.* **2001**, *41*, 189−207.

DOI: 10.1021/acs.langmuir.8b03109
Langmuir 2018, 34, 13713−13724